InP-Based Broadband Photodetectors With InGaAs/GaAsSb Type-II Superlattice

Jingyi Wang, Zhiyang Xie, Liqi Zhu, Xinbo Zou, Xuyi Zhao, Wenfu Yu, Ruotao Liu, Antian Du, Qian Gong, and Baile Chen, *Senior Member, IEEE*

***Abstract*— In this work, an $In_{0.53}Ga_{0.47}As/GaAs_{0.5}Sb_{0.5}$ type-II superlattice(T2SL) based broadband photodetector with an optical spectrum response ranging from 250 nm to 2400 nm is demonstrated. The photodetector shows a low dark current density of 3.48×10^{-4} A/cm^2 under the bias of −1 V and a specific detectivity (D*) of 1.59×10^{10} cm·Hz$^{1/2}$/W at 2 μm at 293 K. A recessed window on the surface of the top P layer was fabricated to enhance the responsivity of ultraviolet (UV) and visible band. The UV and visible band quantum efficiency (QE) can increase by 40% with the recessed window.**

***Index Terms*— Broadband photodetector, InP-based photodetector, InGaAs/GaAsSb type-II superlattice.**

I. Introduction

PHOTODETECTORS have wide applications in the areas such as thermal imaging, chemical sensing, and gas monitoring [1]. Silicon photodetectors have excellent performance in the ultraviolet (UV), visible, and near-infrared region. However, the quantum efficiency of Si photodetectors drops quickly beyond 1000 nm. For the short-wave infrared (SWIR) detection up to 1700 nm, lattice-matched InGaAs on InP photodetectors are well developed with low dark current and high quantum efficiency (QE) performance. To further extend detection wavelength beyond 2000 nm, In-rich InGaAs photodetectors are typically used [2], however, the devices often suffer from dislocation defects that propagate into the active region, which cause a high dark current. InP-based InGaAs/GaAsSb type-II Superlattice (T2SL) is another option to extend the detection wavelength to 3 μm, which is lattice-matched or strain-compensated to InP substrate and could potentially overcome the lattice-mismatch issue of In-rich InGaAs photodetectors [3]–[7]. For multi-spectrum applications, it is desirable to have a single photodetector with broadband photoresponse from UV to extended-SWIR, which could significantly reduce the complexity and cost of the receiver system.

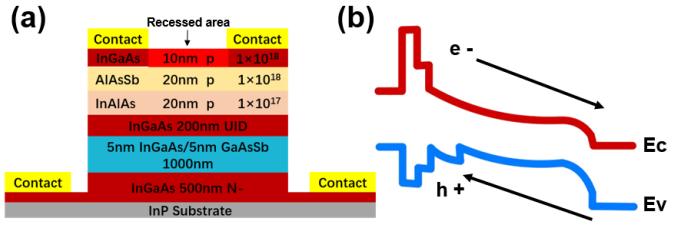

Fig. 1. (a) Layer structure of the broadband photodetector, light red area in the first layer indicates the recessed region in further steps. (b) Band diagram of the broadband photodetector.

Various broadband photodetectors have been studied so far. Lee *et al.* [8] demonstrated a PbS nanocrystal based broadband photodetector that works from 300 nm to 2000 nm with a peak responsivity of 0.21 A/W at 1800 nm. John *et al.* developed a $MoSe_2$–Si heterojunction broadband transition metal dichalcogenide (TMD) with a spectral range from 405nm to 2500nm and a peak detectivity of 6.7×10^9 Jones [9].

This work demonstrated a broadband photodetector with the optical response from UV to the extended-SWIR band based on the InGaAs/GaAsSb T2SL. The previously reported InGaAs/GaAsSb T2SL photodiodes [10]–[12] usually have an optical response from 900 nm to 2500 nm. At the wavelength below 900, the response of the device quickly dropped due to the strong absorption in the p-InP layer. In this work, we use a thin p-layer with larger bandgap AlAsSb/AlInAs materials to minimize the light absorption in the UV/VIS band and allow more light penetrates the depletion region, thus increasing the response in the UV/VIS band to extend the cut-on wavelength. The reported device has been demonstrated with the optical response from 250 nm to 2400 nm at room temperature with a low dark current density of 3.48×10^{-4} A/cm^2 and a peak detectivity of 6.45×10^{10} cm·Hz$^{1/2}$/W. In order to further improve the optical response in the UV/visible side, a recessed window on the top of the device was fabricated, with the QE further enhanced by 40%.

Manuscript received February 28, 2022; revised March 16, 2022; accepted March 22, 2022. Date of publication March 25, 2022; date of current version April 26, 2022. This work was supported in part by the National Key Research and Development Program of China under Grant 2019YFB2203400 and in part by the National Natural Science Foundation of China under Grant 61975121. The review of this letter was arranged by Editor L. K. Nanver. *(Corresponding author: Baile Chen.)*

Jingyi Wang is with the School of Information Science and Technology, Shanghaitech University, Shanghai 201210, China, also with the Shanghai Institute of Microsystem and Information Technology, Chinese Academy of Sciences, Shanghai 200050, China, and also with the Shanghai Engineering Research Center of Energy Efficient and Custom AI IC, Shanghai 201210, China.

Zhiyang Xie, Liqi Zhu, Xinbo Zou, and Baile Chen are with the School of Information Science and Technology, Shanghaitech University, Shanghai 201210, China, and also with the Shanghai Engineering Research Center of Energy Efficient and Custom AI IC, Shanghai 201210, China (e-mail: chenbl@shanghaitech.edu.cn).

Xuyi Zhao, Wenfu Yu, Ruotao Liu, Antian Du, and Qian Gong are with the Key Laboratory of Terahertz Solid State Technology, Shanghai Institute of Microsystem and Information Technology, Chinese Academy of Sciences, Shanghai 200050, China.

Color versions of one or more figures in this letter are available at https://doi.org/10.1109/LED.2022.3162246.

Digital Object Identifier 10.1109/LED.2022.3162246

II. Structure and Fabrication

Figure 1. (a) shows the epitaxial structure of the InP-based broadband photodetector. The epitaxial layer structure was grown by molecular beam epitaxy (MBE) on InP substrate. The epitaxial growth began sequentially with 500 nm n-doped InGaAs, 1000 nm thickness of 5 nm InGaAs/ 5 nm GaAsSb T2SL unintentionally doped (UID) layer, 200 nm InGaAs UID layer. Following the InGaAs UID layer are three p-doped layers, including 20 nm InAlAs, 20 nm AlAsSb and 10 nm InGaAs material. The InGaAs layer is used as the contact layer, the AlAsSb layer is to block the photo-generated electrons diffusing into p-contact, and the InAlAs layer is used to "smooth" the valence band offset between p-region and i-region. The band diagram is shown in Fig.1 (b). The total thickness of the p-layer is very thin to minimize the light absorption in the p-region and allow more light in UV and visible band to penetrate into the depletion region, since the photo-generated carriers in p-layer have a relatively high surface recombination rate and could easily recombine without contributing the photocurrent. After the wafer growth, front-illuminated mesa structures were fabricated by wet etching with $H_3PO_4 : H_2O_2 : H_2O$ solution (1 : 1 : 10). A Ti/Pt/Au metal stack was deposited as both p- and n-type contacts. A 194-nm-thick silicon nitride (SiN_x) anti-reflection layer was deposited on the top of the device as the passivation layer as well.

III. Results and Discussions

A. Material Characterization

The photoluminescent (PL) measurement result at 300K was plotted in Fig.2 (a). The PL signal shows a peak at the wavelength of 2.2 μm, corresponding to an effective band gap of ~0.55 eV. The X-ray diffraction (XRD) ω-2θ scan of the epitaxial wafer sample was shown in Fig.2 (b). It's noticed that there is a slight mismatch between the peak of InP substrate and 0^{th} peak of superlattice, which indicates slight growth deviation from the design of the superlattice.

B. Electrical Characterization

The dark current of the device with different diameters was measured in a low-temperature probe station by a semiconductor device analyzer. A linear relationship between the dark current and the device area indicates that the dark current was dominated by bulk dark current.

The dark current density-voltage characteristics of device at various temperatures ranging from 160 K to 310 K were shown in Fig.3 (a). The dark current density is 1.59×10^{-8} A/cm^2 at 160 K under the -0.5 V bias and 6.11×10^{-8} A/cm^2 under -1 V bias. At room temperature of 293 K, the device shows a dark current density of 1.30×10^{-4} A/cm^2 under -0.5 V bias and 3.48×10^{-4} A/cm^2 under the bias of -1 V. These values are comparable with the previously reported InGaAs/GaAsSb T2SL photodetectors [5], [13] and In-rich InGaAs [2].

The activation energy (E_a) of device under -0.5 V and -1 V was calculated by fitting the temperature dependent dark current density according to the Arrhenius equation, as shown in Fig.3 (b). The linear fit at high temperature regime (220-310 K) yields an activation energy E_{a1} of 340 meV and E_{a3} of 370 meV, higher than the half-effective-bandgap

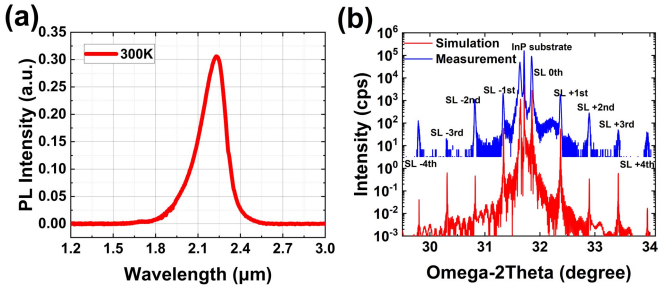

Fig. 2. (a) Photoluminescent measurement result at 300K. (b) XRD ω-2θ scan of the epitaxial wafer sample shown with blue curve, simulation fitting result shown in red.

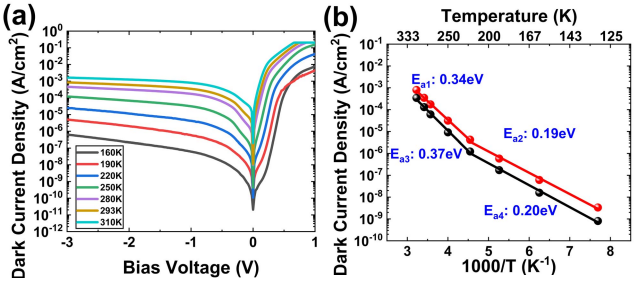

Fig. 3. (a) Dark current density-voltage plot from 160 K-310 K. (b) Arrhenius plot and the linear fits under the bias voltage of -1 V (red) and -0.5 V (black).

(~275 meV), indicating the dark current is dominated by diffusion current and generation-recombination current (G-R). The activation energy E_{a2} and E_{a4} at a lower temperature regime (160-220 K) is 190 meV and 200 meV, suggesting that the other components such tunneling, or surface leakage begin to dominate the dark current.

C. Optics Characterization

The optical characteristics of the broadband photodetector are measured at room temperature. We used a Xenon lamp of 1000W to provide ultraviolet light and a halogen lamp of 360W to generate UV/visible and infrared light for the measurement. Slit size is 7mm. The light passed through a monochromator, and then the monochromatic light was modulated by a 180 Hz chopper and focused on a 180 μm diameter device. Behind the fiber outlet was a concave mirror and a 15× focusing mirror, which converged the divergent light into a ~50 μm spot on the device surface. The photoresponse spectrum from 200 nm to 2500 nm was plotted in Fig.4. The dashed line represents the responsivity of the device under the bias of -0.5V, and the solid line stands for that under -1 V.

Here multiple commercial photodetectors with known response at different bands are used to calibrate the device responsivity. A UV-extended Silicon photodiode (Thorlabs FDS010) was used to measure the response of the device from 200 nm to 400 nm, drawn by blue lines. A standard Silicon detector (Thorlabs FDS1010-CAL) was applied, ranging from 350 nm to 1050 nm, which is drawn with red lines. The responsivity range from 1000 nm to 2500 nm with orange lines was measured by an In-rich InGaAs detector (PDA10DT-EC).

The detector demonstrates a response in a broad spectrum that begins from 250 nm and cuts off at 2400 nm, covering the near-UV, visible light, NIR, and extended-SWIR, which has

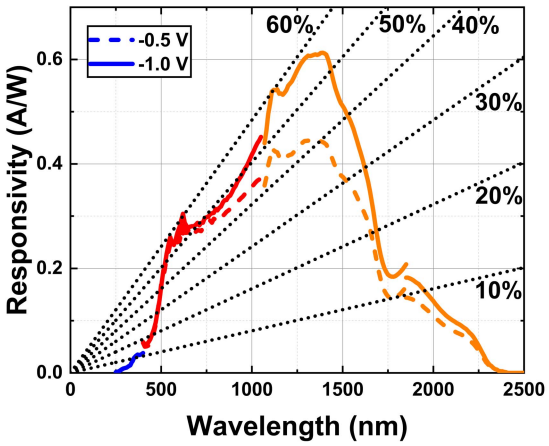

Fig. 4. Responsivity-spectrum the broadband photodetector under −0.5 V and −1 V bias voltage at room temperature of 293 K. (Six black dot line is the quantum efficiency contour plot in the same figure.)

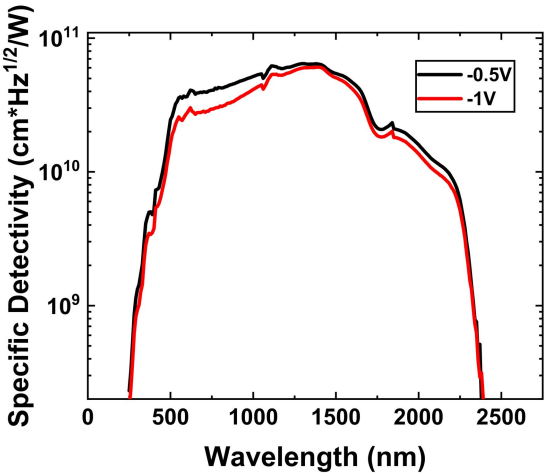

Fig. 5. Specific detectivity measured under the bias of −0.5 V and −1 V at room temperature.

never been demonstrated in any III-V or Si-based photodetectors. The device shows a quantum efficiency of over 40% from 500 nm to 1550 nm under −1 V bias. The anti-reflection coating contributes to the high QE around 1550 nm. The QE of the device is 60.9 % at 620 nm and 60.1 % at 1110 nm. The QE performance of this device is slightly lower than the commercial InGaAs detectors, which can be further enhanced with a thicker InGaAs layer.

The specific detectivity D^* was calculated by:

$$D^* = \frac{R\sqrt{A}}{S_n} \tag{1}$$

where R is the responsivity of the device, S_n is the measured white noise spectrum density, A is the device area.

The calculated specific detectivity was shown in Fig. 5. The device has a D^* of 6.45×10^{10} cm·Hz$^{1/2}$/W at 1310 nm wavelength under −0.5 V bias at room temperature. At wavelength of 2000 nm, the D^* is 1.59×10^{10} cm·Hz$^{1/2}$/W, which is also comparable with the previously reported InGaAs/GaAsSb T2SL photodetectors and other eSWIR photodetectors including HgCdTe and commercial In-rich InGaAs photodetectors at room temperature [5], [9], [14]–[18].

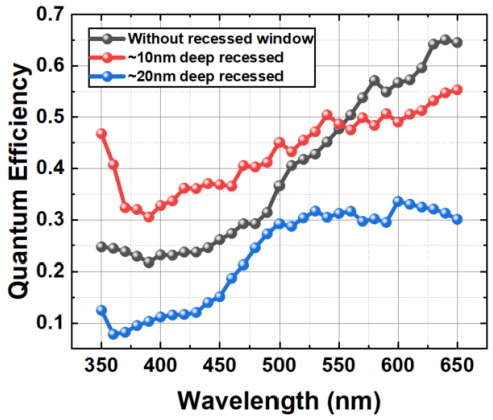

Fig. 6. EQE of the same device before and after opening a recess window with different etching depths on the top p InGaAs region.

Regarding the absorption and the carrier collection efficiency of the top p-type InGaAs contact layer at the UV/visible band, a recessed window structure was used to further enhance the QE in the UV/visible band. The recessed window of the device was formed by further wet etching in $H_3PO_4 : H_2O_2 : H_2O$ solution (1 : 1 : 20) with no AR coating added. The recessed region was indicated in fig1. (a). The etching depth of the recessed window is around 10 nm for the first-time recess window etching process and around 20 nm for the second-time recess window etching process. The results of measured QE from 350 nm to 650nm of the device are plotted in Fig. 6. An improvement of around 40% on QE in UV band is demonstrated for the device with about 10 nm deep recessed window. It is also noted that there is a slight QE reduction from 550 nm to 650 nm. Moreover, QE could degrade significantly if approximately 20 nm thick p-layer is recessed as shown in Fig. 6. That may be due to the reduced electrical field in the depleted region as part of the p-layer is removed.

IV. Conclusion

In conclusion, an InP-based InGaAs/GaAsSb type-II superlattice broadband photodetector is demonstrated in this work. The device shows a dark current density of 3.48×10^{-4}A/cm^2 at room temperature under −1 V bias and has a specific detectivity of 6.45×10^{10} and 1.59×10^{10} cm·Hz$^{1/2}$/W at the wavelength of 1310 nm and 2000 nm, respectively. The device responds to a broadband of incident light starting from 250 nm and cutting off at 2400nm, with a quantum efficiency over 10 % from 350 nm to 1960 nm. A recessed window on the surface P region is fabricated. The device with a recessed window shows a 40% QE improvement compared to that without a recessed window. There are still some future works that can be done to further improve the responsivity at eSWIR and UV band such as increasing the thickness of T2SLs layer or using InP as the p-cap layer.

References

[1] P. Martyniuk, J. Antoszewski, M. Martyniuk, L. Faraone, and A. Rogalski, "New concepts in infrared photodetector designs," *Appl. Phys. Rev.*, vol. 1, no. 4, 2014, Art. no. 041102.

[2] Y. Ma, X. Li, X. Shao, S. Deng, J. Cheng, Y. Gu, Y. Liu, Y. Chen, X. Zhu, T. Li, Y. Zhang, H. Gong, and J. Fang, "320 × 256 extended wavelength $In_xGa_{1-x}As$/InP focal plane arrays: Dislocation defect, dark signal and noise," *IEEE J. Sel. Topics Quantum Electron.*, vol. 28, no. 2, pp. 1–11, Mar. 2022, doi: 10.1109/JSTQE.2021.3087182.

[3] B. Chen, W. Y. Jiang, J. Yuan, A. L. Holmes, and B. M. Onat, "Demonstration of a room-temperature InP-based photodetector operating beyond 3 μm," *IEEE Photon. Technol. Lett.*, vol. 23, no. 4, pp. 218–220, Feb. 15, 2011, doi: 10.1109/LPT.2010.2096205.

[4] B. Chen, W. Jiang, J. Yuan, A. L. Holmes, and B. M. Onat, "SWIR/MWIR InP-based p-i-n photodiodes with InGaAs/GaAsSb type-II quantum wells," *IEEE J. Quantum Electron.*, vol. 47, no. 9, pp. 1244–1250, Sep. 2011, doi: 10.1109/JQE.2011.2160450.

[5] R. Sidhu, N. Duan, J. C. Campbell, and A. L. Holmes, "A long-wavelength photodiode on InP using lattice-matched GaInAs-GaAsSb type-II quantum wells," *IEEE Photon. Technol. Lett.*, vol. 17, no. 12, pp. 2715–2717, Dec. 2005.

[6] Z. Xie, Z. Deng, X. Zou, and B. Chen, "InP-based near infrared/extended-short wave infrared dual-band photodetector," *IEEE Photon. Technol. Lett.*, vol. 32, no. 16, pp. 1003–1006, Aug. 15, 2020.

[7] Y. Chen, Z. Xie, J. Huang, Z. Deng, and B. Chen, "High-speed uni-traveling carrier photodiode for 2 μm wavelength application," *Optica*, vol. 6, no. 7, pp. 884–889, 2019.

[8] J. W. Lee, D. Y. Kim, S. Baek, H. Yu, and F. So, "Inorganic UV–visible–SWIR broadband photodetector based on monodisperse PbS nanocrystals," *Small*, vol. 12, no. 10, pp. 1328–1333, Mar. 2016, doi: 10.1002/smll.201503244.

[9] J. W. John, V. Dhyani, S. Maity, S. Mukherjee, S. K. Ray, V. Kumar, and S. Das, "Broadband infrared photodetector based on nanostructured $MoSe_2$–Si heterojunction extended up to 2.5 μm spectral range," *Nanotechnology*, vol. 31, no. 45, Nov. 2020, Art. no. 455208, doi: 10.1088/1361-6528/ab95b9.

[10] K. Sugimura, T. Go, T. Fuyuki, T. Kawahara, H. Inada, and Y. Iguchi, "High-performance extended SWIR photodetectors using strain compensated InGaAs/GaAsSb type-II quantum wells," *Proc. SPIE*, vol. 10926, Feb. 2019, Art. no. 109260E.

[11] J. Easley, C. R. Martin, M. H. Ettenberg, and J. Phillips, "InGaAs/GaAsSb type-II superlattices for short-wavelength infrared detection," *J. Electron. Mater.*, vol. 48, no. 10, pp. 6025–6029, Oct. 2019, doi: 10.1007/s11664-019-07441-x.

[12] J. Yuan, B. Chen, and A. Holmes, "Near-infrared quantum efficiency of uncooled photodetectors based on InGaAs/GaAsSb quantum wells lattice-matched to InP," *Electron. Lett.*, vol. 47, no. 20, pp. 1144–1145, 2011.

[13] T. Kawahara, K. Machinaga, B. Sundararajan, K. Miura, M. Migita, H. Obi, T. Fuyuki, K. Fujii, T. Ishizuka, H. Inada, and Y. Iguchi, "InGaAs/GaAsSb type-II quantum-well focal plane array with cutoff-wavelength of 2.5 μm," *Proc. SPIE*, vol. 10111, Jan. 2017, Art. no. 1011115.

[14] *In-Rich InGaAs PIN*. Accessed: Feb. 2022. [Online]. Available: https://www.hamamatsu.com/jp/en/product/type/G12183-210KA-03/index.html

[15] J. Rothman, L. Mollard, S. Bosson, G. Vojetta, K. Foubert, S. Gatti, G. Bonnouvrier, F. Salveti, A. Kerlain, and O. Pacaud, "Short-wave infrared HgCdTe avalanche photodiodes," *J. Electron. Mater.*, vol. 41, no. 10, pp. 2928–2936, Oct. 2012, doi: 10.1007/s11664-012-1970-4.

[16] K. Sugimura, T. Go, T. Fuyuki, T. Kawahara, H. Inada, and Y. Iguchi, "High-performance extended SWIR photodetectors using strain compensated InGaAs/GaAsSb type-II quantum wells," *Proc. SPIE*, vol. 10926, Feb. 2019, Art. no. 109260E.

[17] C. Jin, F. Wang, Q. Xu, C. Yu, J. Chen, and L. He, "Beryllium compensation doped InGaAs/GaAsSb superlattice photodiodes," *J. Cryst. Growth*, vol. 477, pp. 100–103, Nov. 2017.

[18] Y. Uliel, D. Cohen-Elias, N. Sicron, I. Grimberg, N. Snapi, Y. Paltiel, and M. Katz, "InGaAs/GaAsSb type-II superlattice based photodiodes for short wave infrared detection," *Infr. Phys. Technol.*, vol. 84, pp. 63–71, Aug. 2017, doi: 10.1016/j.infrared.2017.02.003.